ASGE Vol. 03 (01), pp. 40-51, 2022

Egyptian Knowledge Bank

International Journal of Advances in Structural and Geotechnical Engineering

https://asge.journals.ekb.eg/

Print ISSN 2785-9509 Online ISSN 2812-5142

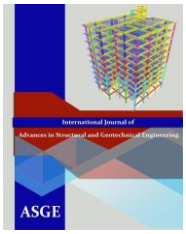

ANALYSIS OF EXTERNALLY PRESTRESSED SEGMENTAL BOX GIRDERS UNDER BENDING, SHEAR, AND TORSION

Mahmoud Abdel-Aziz[1], Tarek El-Shafiey[2], Abdel-Hakeem Khalil[3], Emad Etman[4], Mohammed Hussein[5]

[1]Assistant Professor, Faculty of Engineering, Tanta University, Egypt (corresponding Author)
Tele: 0201008817447, email: mahmoud.abdelaziz@f-eng.tanta.edu.eg
[2,3,4,5]Professor, Structural Engineering Department, Faculty of Engineering, Tanta University, Tanta, Egypt

ABSTRACT

Analysis of Externally Prestressed Segmental Bridges (EPSBs) still needs more effort. At an earlier stage, an experimental investigation was carried out by the authors. The experimental investigation was consisted of ten specimens having different joint configurations, and it was divided into two phases. The first phase contains five specimens constructed with multiple small-amplitude shear keys in accordance with AASHTO. The parameters selected for the first phase were different levels of prestressing force in tendons as well as different levels of applied torsion. The second phase contained four segmental specimens and a monolithic one. The joints in the second phase took four forms: multiple small-amplitude shear keys, large-reinforced shear key, steel shear connectors, and UHP–SHCC joint connecting the tension flange. This paper proposed an analytical procedure to calculate the full prestressing load and partial prestressing load based on the forces' equilibrium. Skew Bending Model that inspected by Huan and Liu, 2006, to calculate the load-carrying capacity for segmental beams with internal unbonded tendons subjected to combined bending, shear, and torsion modified to calculate the ultimate capacity of EPSBs and gave satisfactory agreement with the experimental results.

Keywords: Analysis; Prestressed; Segmental; Bending; Shear; Torsion

NOTATIONS

M	the external applied bending moment
Q	the external applied shear force
M_t	the external applied torsional moment
A_{ps}	the area of tendons at one side.
α	the tendon inclination
f_{yp}	the yield stress of Prestressing tendons
s	the distance between the web bars
f_y	the yield stress of the web bars and tension internal steel
A_{key}	the minimum area of the base of all shear keys in the failure plane.
σ_n	the average compressive stress across

h'	The internal stirrups width height
N	effective tendon forces
A_o	the closed area of centerline thickness
t	the thickness of cross section
v_s	shear stress due to shear force
v_t	shear stress due to torsion
e	the tendon eccentricity
P_{sl}	the prestressing force divided by the yielding force (Prestressing level)
$M_{t,co,s}$	strengths in torsion of the segmental girder
$M_{co,s}$	strengths in bending of the segmental

Article history: Received January 2022 & Accepted February 2022
DOI: 10.21608/ASGE.2022.152821.1021

	the joint
A_{sm}	the area of contact between smooth surfaces in the failure plane.
f_{cu}	the characteristic concrete compressive strength.
h	the distances between the external tendons and the compression internal reinforcements
$Q_{co,m}$	strengths in shear of the monolithic girder
b'	The internal stirrups width

	girder
$Q_{co,s}$	strengths in shear of the segmental girder
$M_{t,co,m}$	strengths in torsion of the monolithic girder
$M_{co,m}$	strengths in bending of the monolithic girder
UHP-SHCC	Ultra-High Performance-Strain Hardening Cementitious Composites
A_{str}	the area of web bar.

INTRODUCTION

Externally Prestressed Segmental Bridges (EPSBs) had become a preferred construction method for constructing bridges, especially in elevated highway bridges. The prestressing tendons may be internally; fully bonded or unbonded, but recently, external prestressing tendons had been widely used, because it offers many advantages. It allows; easily replacement of deteriorated concrete segments or tendons, monitoring the tendons during post-tensioning, shorter construction time due to independence of concreting and prestressing, simple elements assembly in the site. Externally prestressed technique also used for strengthening existing bridges, Algorafi et al. [1].

Kordina et al. [2] and Falkner et al. [3] investigated experimentally the influence of a combined shear, bending, and torsion on the behavior of segmental structures. Huang and Liu [4] presented a modified skew bending model. It could calculate the capacity of prestressed segmental beams with internal unbonded tendons subjected to combined forces. The model gave satisfactory results against the test results of Kordina et al. [3] and Falkner et al. [4]. The equations were built on the premise that yielding of the internal and main prestressing reinforcements in segmental girder has occurred. The load-carrying capacity may be achieved by substituting in the interaction equation no. 4 with the strengths calculated from equations no. 1, 2, and 3.

1. $M_{co,s} = \left(2\left(A_{ps}.f_{yp}\right).h\right)$
2. $Q_{co,s}^2 = \frac{8}{3}.h.\left(A_{ps}.f_{yp}\right).\left(\frac{A_{str}.f_y}{s}\right)$
3. $M_{t,co,s}^2 = 2h.\left(A_{ps}.f_{yp}\right).\left(\frac{A_{str}.f_y}{s}\right).b'^2$
4. $\frac{M}{M_{co,s}} + \left(\frac{Q}{Q_{co,s}}\right)^2 + \left(\frac{M_t}{M_{t,co,s}}\right)^2 = 1$

Where: $M_{t,co,s}$, $M_{co,s}$, $Q_{co,s}$ are the single strengths in torsion, in bending and in shear for a segmental girder; M, Q, M_t are the straining actions bending, shear and torsion due to external load. h is the distances between the external tendons and the compressed internal reinforcements. f_y is the yield stress of the web steel and tension internal steel. f_{yp} is the yield stress of prestressing tendons. s is the distance between the web steel. A_{str} is the area of web steel.

Algorafi et al. [5, 6, 7, and 8] studied the behavior of EPSBs under a combined moment, shear and torsion. The effect of different external tendon layouts, types of joints between segments,

and different levels of torsional force were investigated. The following equation was suggested by Algorafi et al. [8] to calculate the capacity of EPSBs under shear and torsion:

5. $\mathrm{v_c} = (0.585 \times \mathrm{A}_{sm} \times \sigma_n) + A_{key} \times \sqrt{f_{cu}} \times (0.453 \times \sigma_n + 0.574) + 2\mathrm{N} \times \sin \propto$

Where: σ_n is the average compressive stress across the joint (MPa). A_{sm} is the area of contact between smooth surfaces in the failure plane (mm^2). f_{cu} is the characteristic concrete compressive strength (MPa). A_{key} is the minimum area of the base of all shear keys in the failure plane (mm^2). α is the tendon inclination. N is the average tendon force (kN). Then, the applied shear can be calculated from equations 6, 7 and 8

6. $\mathrm{v_s} = \frac{Q}{A_{sm}}$
7. $V_t = \frac{Mt}{2 * A_o * t_e}$
8. $\mathrm{v_c} = \mathrm{v_s} + V_t$

Where: A_o is the closed area of centerline thickness. t is the thickness of cross section. v_s is the shear stress due to shear force. v_t is the shear stress due to torsion. Q is the shear force. M_t is the torsion.

The capacity of EPSBs calculated by the previous models in the case of external tendons may be inaccurate. Huang and Liu's [4] model was constructed to get the capacity of the segmental girders with internal tendons only. The capacity of cross sections with internal tendons is greater than the capacity of cross sections with external tendons because internal tendons cross the joints and will contribute to increasing the capacity by dowel effect. The Model constructed by Algorafi et al. [8] is used to calculate the capacity for (EPSBs) failed by sliding or twisting at the joints only. Capacity recorded by Algorafi et al. [5, 6, 7, and 8] did not express the actual capacity of (EPSBs) because the shear keys between sections were failed by shear stresses. Hence, the capacity computed by this model reflects the shear keys capacity. For these reasons, this paper was conducted to discuss the analysis of distinctive loads points in load-deflection curves of EPSBs subjected to combined bending, shear, and torsion. It has been founded that the load-deflection for segmental specimens went through five stages up to failure: balancing load, full prestressing load, shear keys resisting load, partial prestressing load, and ultimate load. In this paper, analysis of every load was carried out, as well as analytical model based on Huang and Liu's [4] model have been proposed to calculate the ultimate capacity of (EPSBs)

EXPERIMENTAL WORK AND LOAD DEFLECTION BEHAVIOR OBTAINED BY AUTHORS, EL-SHAFIEY ET AL., [11, AND 12]

At an earlier stage, the authors conducted an experimental investigation to study the structural behavior of EPSBs. Different levels of prestressing forces, P^i, in tendons were as: $0.26f_{ys}$, $0.38f_{ys}$ and $0.5f_{ys}$, where f_{ys} is the yield strength. Different levels of torsional moments were introduced by changing the applied load eccentricity, e, as follows: e= 50, 200 and 400mm from the specimen centerline. Four configurations of shear keys were constructed at joints as follows: multiple small amplitude shear keys in accordance with AASHTO 2010, large-reinforced shear key, steel shear connectors and large reinforced shear key in addition to UHP-SCC joining the tension flange.

Figures 1 and 2 show load-deflection curves of tested specimens. It was cleared that the load-deflection curves passed through two trends; Initially, the structural response was linear and under load increase the joint opened, then the stress in external tendons started to increase and the behavior became nonlinear up to failure. It was noticed that both monolithic and segmental specimens exhibited approximately the same behavior till joints started to open, then the behavior became different. Specimens SCN and UHP-S were constructed with steel shear connectors and UHP-SCC joint joining the tension flange respectively, showed better or similar behavior if it is compared with the monolithic specimen, M. It was observed that load-deflection curves for these specimens passed through three stages. Initially, structural responses were linearly, and with a load increased stresses increased in external tendons resulting in a nonlinear stage and the last trend is affected by yielding of internal steel up to failure. Every loading stage was noticed from the experimental results described in Table 1, as follows: load at fully reversed cumber (balancing load); load at the joint opening (full prestressing load); load at the increase in external tendon's stress (partial prestressing load); failure load (ultimate capacity). An idealized load-deflection-curve shown in Figure 3 is proposed for segmental specimens to simulate with studied experimentally specimens.

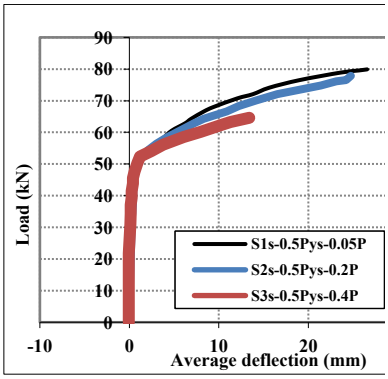

Specimens of group GI

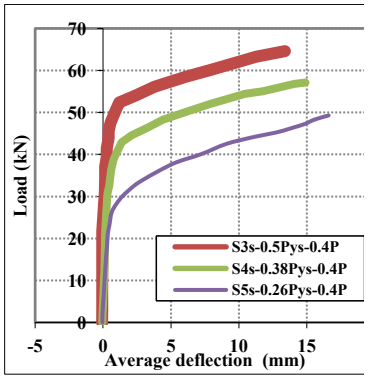

Specimens of group GII

Fig. 1. The load -average deflection, El-Shafiey et al., [11]and Abdelaziz, [9]

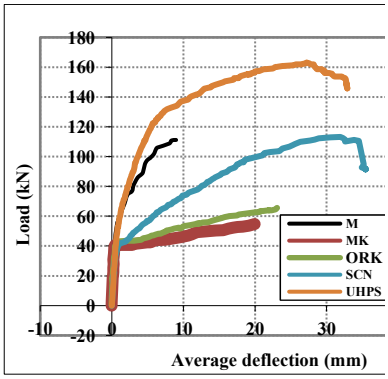

Figure 2. The load -average deflection, El-Shafiey et al., [12] and Abdelaziz, [9]

Table 1: Description of tested specimens and results conducted by authors

Reference	Groups		specimen	L* (mm)	Joint types	Pi	e (m)	P_{bal} (kN)	$P_{f.p}$ (kN)	$P_{p.p}$ (kN)	P_u (kN)
El-Shafiey et al. [11]	GI		S1	1100	Multiple small amplitude shear keys	$0.5P_{ys}$	0.05 m	14.7	42	49	79.9
			S2	1100		$0.5P_{ys}$	0.20 m	14.7	42.5	49.5	77.86
		GII	S3	1100		$0.5P_{ys}$	0.40 m	14.7	42	49	64.6
			S4	1100		0.38 P_{ys}	0.40 m	11.5	32.6	38.76	57
			S5	1100		0.26 P_{ys}	0.40 m	7.5	22.18	26.54	49.3
El-Shafiey et al. [12]			M	800	Monolithic	0.26 P_{ys}	0.40 m	7.5	42.25	58	111
			MK	800	Multiple small amplitude shear	0.26 P_{ys}	0.40 m	7.5	40	40	54.7

			keys						
	ORK	800	Large-reinforced shear key	0.26 P_{ys}	0.40 m	7.5	40	40	66
	SCN	800	Bonded steel shear connectors	0.26 P_{ys}	0.40 m	7.5	40	40	111.2
	UHP-S	800	Large-reinforced shear key and UHP-SCC joint joining the tension flange	0.26 P_{ys}	0.40 m	7.5	48.25	60	162.8

L* is the distance between the first joint and the applied load (mm), $\mathbf{P_i}$ Prestressing force level calculated as a ratio from the yield force. **e** is the applied force eccentricity. $\mathbf{P_{bal}}$, $\mathbf{P_{f.p}}$, $\mathbf{P_{p.p}}$ **and** $\mathbf{P_u}$ are balanced, partial, full prestressing and ultimate loads, respectively.

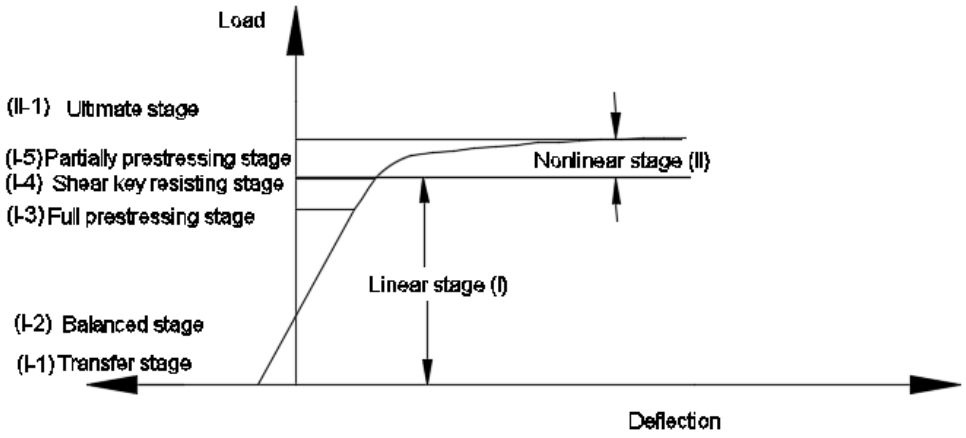

a. Idealized Load-deflection curve

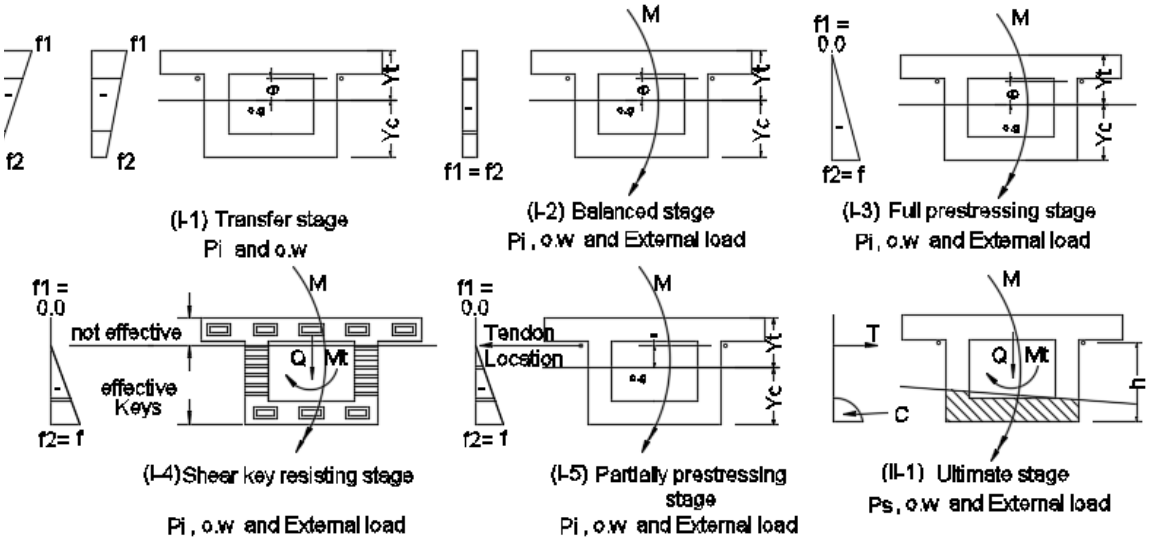

b. Different loading stages up to failure

Fig. 3. Idealized Load-deflection curve and different loading stages up to failure

Pilot specimens of El-Shafiey et al. [11] may be early collapsed and the actual ultimate load couldn't be recorded, perhaps due to the vicinity of the first joint to the fixed base. This leads to an unclear failure envelope. Specimens of El-Shafiey et al. [11] were constructed to treat the defects that happened for specimens of El-Shafiey et al. [9]. The first joint distance from the fixed base is increased to have a clear failure envelope. The specimen uses also different joint configurations; steel shear connectors in SCN and was connected with sufficient embedded length at the joints. Due to low clearance between shear connectors with its female which lead to limit the movement at the first joint, multi joints were opened which led to increasing the flexural capacity. Also, additional stirrups which added to eliminate the concentration of stress at the edge connectors led to increasing the shear strength. Finally, the overall capacity is improved, and the specimen achieved the monolithic specimen, M, in the ultimate load. Also, the specimen incorporates large, reinforced shear keys and UHP-SCC joint which has high ductility and tensile strength connected segment at the tension flange, gives ultimate load exceeded that of the monolithic specimen due to connecting the steel area at tension zone and contribution of fibers in increasing the flange tensile strength as well as the contribution of the additional steel around shear keys to increase the shear capacity.

ANALYSIS OF EPSBS FOR ALL STAGES UNTIL FAILURE

As mentioned before EPSBs pass through various stages up to failure as follows: stage 1) transfer stage, stage 2) balanced stage, stage 3) full prestressing load, stage 4) shear keys resisting stage, stage 5) partial prestressing load, stage 6) ultimate load. The first five stages are linear, and the nonlinear stage is occurring after point no. 5 up to failure. The compressive stress resulted from the prestressing at first three stages, reduces the effect of the torsion on the specimen. Therefore, the torsion is neglected in the analysis of stages 1,2, and 3. The normal stress due to torsional warping is neglected at the linear stage because the box section has enough torsional rigidity and only normal stress due to moment will be considered. Where specimens of El-Shafiey et al. [11] didn't achieve their ultimate loads, thus it will be included in the analyses for the linear stage only. Transfer stage starts after applying external Prestressing, the initial prestressing force led the specimen to camber

Analysis of the Balancing stage

When the normal at the first joint resulting from the prestressing force is balanced with the normal stresses from the external load, the chamber is fully recovered. The stress at this stage is uniform compression. Figure 3 (I–2) shows a uniform compressive stress ($f_1=f_2$). Stresses f_1 and f_2 can be calculated from normal stress equations as follows:

9. $f_1 = -N.\cos\alpha /A - N.\cos\alpha.\, e.\, y_t/Ix + M\, y_t/Ix$
10. $f_2 = -N.\cos\alpha /A + N.\cos\alpha.\, e.\, y_c/Ix - M\, y_c/Ix$

Where, f_1 is the pre-compressed tensile stress. f_2 is pre-tensile compression stress. α is the tendon inclination angle. N is the tendons force, e is the tendon eccentricity, and y is the distance between center of gravity of the section and the point of calculated stress. M is the external bending moment.

By substituting in equations 9 and 10 and putting $f_1=f_2$ then the applied load P_{app} can be calculated. Table 2 shows the experimental finding of balanced load as the comparison with the analytical balanced load. The normal stress equations show good agreement with experimental results.

Analysis of the full prestressing stage

The full prestressing load occurs when the normal stress resulting from the external load and prestressing is equal to zero at the tension side. Figure 3 (I-3) shows the stress at the full prestressing stage. Equilibrium of external and internal action shown in figure 6 is the way to analyze this stage. The external applied force is calculated form the proposed flow chart shown in figure 4.

Where: F_i is the internal forces calculated from the stress distribution. N cos α is the component of tendon's force. X_i is the distance between every internal force F_i and compression side. Y_c is the distance between the section c.g and the compression side. E is the tendon eccentricity. M is the applied external moment. Table 2 shows the experimental full prestressing load in, kN, vs. analytical full prestressing load in, kN, calculated by forces equilibrium. The suggested procedure shows good agreement with experimental results as shown in Table 2.

Analysis of the shear key resisting stage

After full prestressing stage, the dry joint is just to open as shown in Figure 3 (I–4). The bending moment will open the joint, the contacted shear keys and the compressed areas will transfer shear due to shearing force and shear flow due to torsion through the joints. The uncontacted tension zone will be free to twist and there is no force flow through it. By analyzing the force on the shear keys from the balanced stage up to failure, the critical case is that analyzed before the partial prestressing stage. From Figure 5, by neglecting the contribution of shear keys in tension side and calculating the actual force on the interlocked shear keys in webs and compression flange. The factor of safety against failure can be calculated at the most critical shear key (which have maximum r and at the web near the applied load) from the equation:

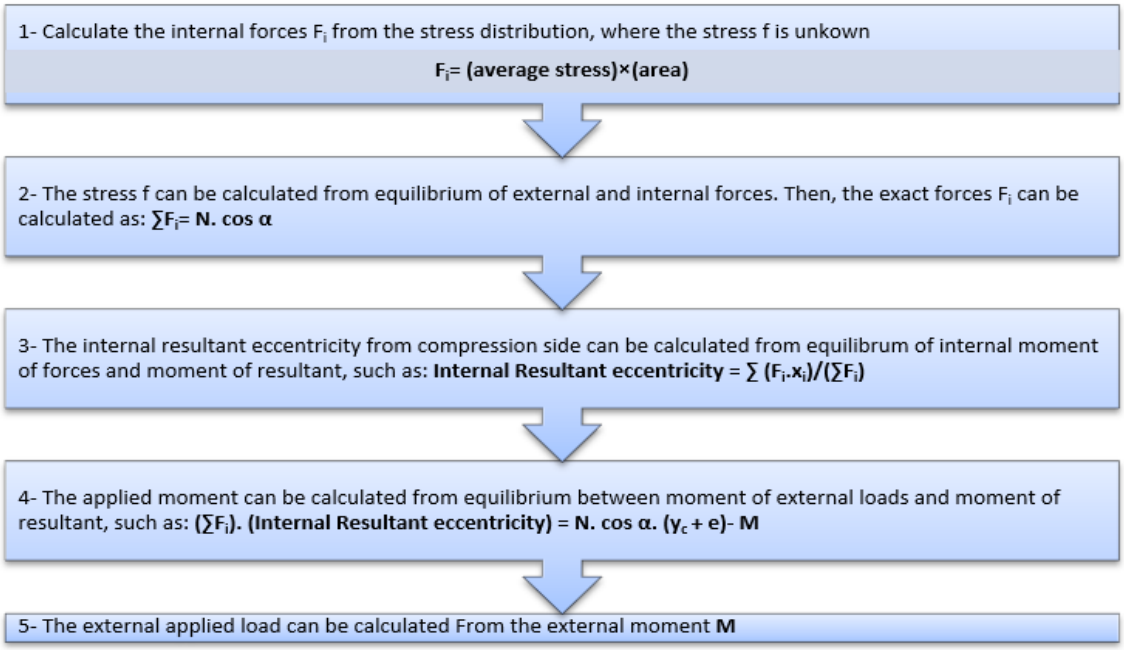

Fig. 4. Flow chart for calculating external applied load for segmental specimens with dry joints at linear stage

11. $F_{ac} = \sqrt{\left(\frac{M_t.y}{\sum r_i^2}\right)^2 + \left(\frac{Q}{N} + \frac{M_t.x}{\sum r_i^2}\right)^2}$ and $F_{all} = A_k \cdot \sqrt{f'_c}.(0.2048 \cdot \sigma_n + 0.9961) + 0.6 \cdot A_{sm} \cdot \sigma_n$

Where F_{ac} is the applied force on shear keys and F_{all} is the allowable force, M_t is the torsional moment, Q is the shearing force, N is the number of shear keys, r_i is the distance between every shear key and centroid of all center of shear keys. X and y are the ordinates of the shear key meagered from the c.g. A_k is the area of the shear key at the failure plane. f_c is the concrete characteristic compressive strength. σ_n is the average compressive stress at shear key calculated at the partial prestressing stage. A_{sm} is contact area around the shear key.

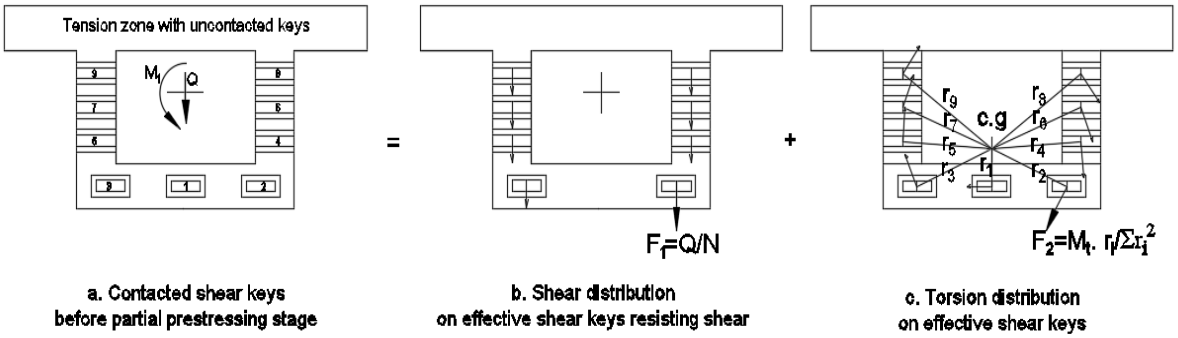

Fig. 5. Shear and torsion distribution on effective shear keys

Analysis of the partial prestressing stage

Figure 3 (I–5) shows the stress at the partial prestressing stage. At this stage, the strain in external tendons is just increase in nonlinear behavior. The procedures given in flow chart shown in Figure 4, may applied on that stage. The normal stress at tendon's location is considered equal to zero. Table 2 shows experimental and analytical partial prestressing loads for different specimens of phase I. Analytical results show good agreement with the experimental finding.

Table 2: Experimental balanced load vs. balanced analytical load

Specimen	Balanced load (kN)		Full prestressing load (kN)		Partial prestressing load (kN)	
	Experimental	Analytical	Experimental	Analytical	Experimental	Analytical
S1	14.7	14.73	42.5	42	49.5	49
S2	14.7	14.73	42	42	49	49
S3	14.7	14.73	42.5	42	49.5	49
S4	11. 5	11.15	32.6	31.8	38.76	37.4
S5	7.5	7.55	22.18	21.5	26.54	26.4

Analysis of the ultimate stage

This stage is occurring when the maximum capacity of specimen is achieved. From results of El-Shafiey et al. [12], specimens ORK and MK failed in the same mode as modified skew bending failure for segmental girders as shown in Figure 6. At the failure plane, it produces a set of internal forces as shown in the figure, where:

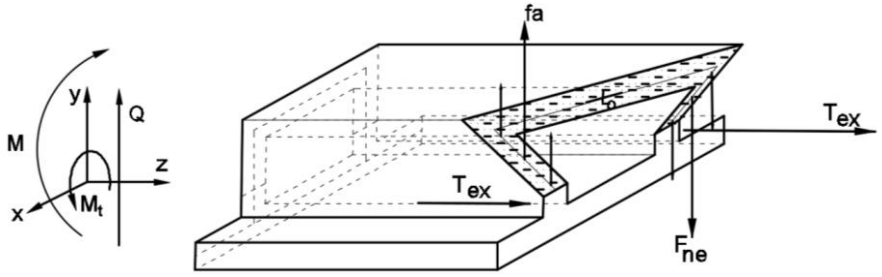

Fig. 6. Free body diagram for segmental specimens MK and ORK in El-Shafiey et al. [12].

F_{ne} is the internal web force near to the applied load. F_{fa} is the internal web force far from the applied load. T_{ex} is the longitudinal force applied at tendons.

Also, failures of specimens UHP-S, SCN and M were similar to mode as skew bending failure for monolithic girders as shown in Figure 7. At the failure plane, it produces a set of internal forces as shown in the figure, where:

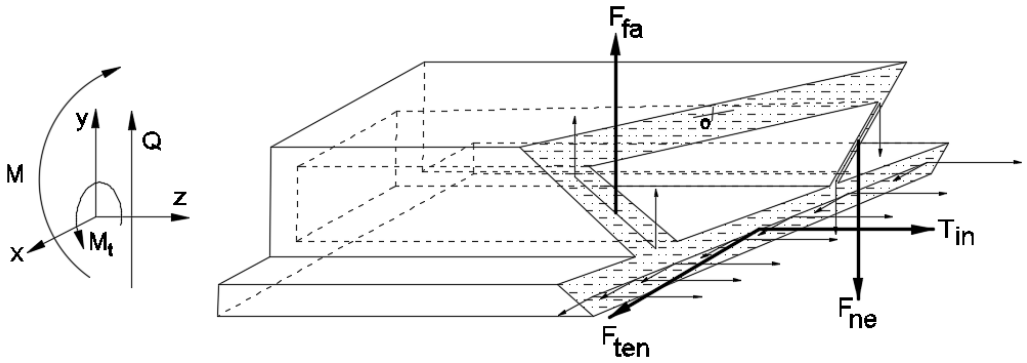

Fig. 7. Failure mode for segmental specimens UHP-S, SCN and M tested by the authors.

F_{ne} is the internal web force near to the applied load. F_{fa} is the internal web force far from the applied load. F_{ten} is the internal web force at the tension flange. T_{in} is the longitudinal force applied at the longitudinal internal reinforcement at the tension flange. T_{ex} is the longitudinal force applied at the external tendon. Based on proposed model by Huang and Liu [4], an analytical model is suggested to calculate the capacities of specimens M, MK, ORK and UHP-S, SCN of segmental box girders with external prestressing under combined straining actions bending, shear and torsion, as follows:

Ultimate capacity of the segmental specimens based on Huang and Liu [4]:

Depending on the magnitudes of the torsion, bending, and shear, the free body diagram can be drawn and the strength equations of Huang and Liu [4] can be deduced. Using free nonlinear regression analysis get the following coefficient that considered nonyielding of external tendons, as follows:

12. Correction of tendon stress, $cofficent = 1.08\sqrt{2P_{s.l}}$

where, $P_{s.l}$ is the prestressing force divided by the yielding force.
It means that the following interaction formulas take the nonyielding of external tendons into consideration, such as:

13. $M_{co.s} = 1.08\sqrt{2.\,\mathrm{P_{s.l}}} \times \left(2\left(\mathrm{A_{ps}} \times \mathrm{f_{yp}}\right) \times \mathrm{h}\right)$

14. $\mathrm{Q_{co.s}^2} = \frac{8}{6} \times \mathrm{M_{co.s}} \times \left(\frac{\mathrm{A_{str}.f_y}}{\mathrm{s}}\right)$

15. $M_{t.cos}^2 = M_{co.s} \times \left(\frac{A_{str}.f_y}{s}\right) \times b'^2$

16. $\frac{M}{M_{co.s}} + (\frac{Q}{Q_{co.s}})^2 + (\frac{M_t}{M_{t.cos}})^2 = 1$

Where, $M_{co,s}$, $Q_{co,s}$ and $M_{t,\ cos}$ are single strength in bending, in shear and in torsion for segmental girders

By calculating the ultimate moment capacity from equation 13 taken the nonyielding into consideration, the ultimate shear capacity from equation 14 and the ultimate torsion capacity from equation 15, then applying in the interaction equation 16, the applied external load can be calculated. Table 3 shows the variation of proposed model and experimental results. The closed form equation based on modified skew bending failure for segmental girders shows good agreement with experimental results.

Table 3: Comparison between experimental and proposed model loads

specimen	Experimental load (kN)	proposed model Load (kN)	variation %
MK	54.7	50.6	-7.4
ORK	66	69	+4.5

3.5.2. Ultimate capacity of the monolithic behavior specimens based on Huang and Liu [4]:

Depending on the magnitudes of the torsion, bending, and shear, the free body diagram can be drawn and the strength equations of Huang and Liu [4] can be deduced. By involving the internal steel into the strength equation of moment, the resulting equations become:

17. $M_{co.m} = \left(2\left(A_{ps} \times f_{yp}\right) \times h\right) + n \times A_s \times f_y + A_{UHP} \times F_t$

18. $Q_{co.m}^2 = \frac{8}{6} \times M_{cos} \times \left(\frac{A_{str} \times f_y}{s}\right)$

19. $M_{t.co.m}^2 = M_{cos} \times \left(\frac{A_{str} \times f_y}{s}\right) \times b'^2$

20. $\frac{M}{M_{co.m}} + (\frac{Q}{Q_{co.m}})^2 + (\frac{M_t}{M_{t.co.m}})^2 = 1$

Where: $M_{t,co,m}$, $M_{co,m}$, $Q_{co,m}$_single strengths in torsion, in bending and in shear for the girder; M, Q, M_t are the applied straining actions bending, shear and torsion. h is the distances between the external tendons and the compression internal reinforcements. f_y is the yield stress of the web bars and tension internal steel. f_{yp} is the yield stress of prestressing tendons. s is the distance between the web bars. A_{str} is the area of web bar. n. A_s is the total main internal tension steel. A_{UHP} is the area of UHP-SHCC joint. F_t is the tensile strength of UHP-SHCC cylinder.

Calculate the ultimate moment capacity from equation 17 neglecting the term $A_{UHP} \times F_t$ for specimen M that introduce the UHP-SHCC capacity. For specimen SCN neglect terms of $n \times A_s \times f_y + A_{UHP} \times F_t$ that introduce the internal tension steel capacity and UHP-SHCC capacity. The applied external load is calculated by determining the ultimate capacity for moment, shear, and torsion from equations 17, 18 and 19, respectively, then compensation in the interaction equation 20. Table 4 shows the variation of loads obtained from the proposed model and experimental results. The closed form equation based on skew bending failure for monolithic girders shows good agreement with experimental results. The large difference between the calculated load of the experimental results and the proposed model of the specimen SCN is due to low clearance between shear connectors with its female which lead to limit movement during bending and twisting moment resulting in opening of multi joints and increasing in specimen capacity.

Table 4: Comparison between experimental and proposed model loads

specimen	Failure load (kN)	proposed model Load (kN)	variation %
M	111	103.5	-6.8
SCN	111	87	-21
UHP-S	162.8	151	-7.2

CONCLUSIONS

1. Suggested methods based on forces equilibrium is used to calculate the loads at the full prestressing stage and the partial prestressing stage. They show good agreement with the experimental results.
2. The modified model based on modified skew bending failure for segmental beams is presented to calculate the ultimate capacity for EPSBs under combined straining actions. It shows a good agreement with the experimental results.
3. The modified closed form equation based on skew bending failure for monolithic beams is presented to calculate the ultimate capacity for EPSBs with steel shear connector joint or UHP-SHCC joint under combined straining actions. It shows a good agreement with the experimental results.

ACKNOWLEDGEMENTS

The authors would like to thank the staff at the Reinforced concrete laboratory and heavy Structures ,at Faculty of Engineering, Tanta University, for their technical help during the experimental program. Finally, the first author would like to acknowledge; Prof. Dr. Tarek El-Shafiey, Prof. Dr. Abdel Hakeem Khalil, Prof. Dr. Emad Etman and Prof. Dr. Mohammed Hussein for their in-depth contribution in the research.

REFERENCES

1. AlGorafi MA, Ali AAA, Jaafar MS, Othman I. (2007) “Performance of segmental prestressed concrete bridges under combined stresses”: a critical review. World engineering congress—CS50.
2. Kordina K, Teutsch M, Weber V. (1984) “Spannbetonbauteile in segmentbauart under kombinierter beanspruchung aus torsion, biegung und querkraft”. J DafStb; 350:5–25.
3. Falkner H, Teutsch M, Huang Z (1997). “Segmentbalken mit vorspannung ohne verbund unter kombinierter beanspruchung aus torsion, biegung und querkraft”. J DafStb; 472:7–50.
4. Huang Z, Liu XL (2006). “Modified skew bending model for segmental bridge with unbonded tendons”. J Bridge Eng, ASCE;11(5):9–63.
5. AlGorafi MA, Ali AAA, Jaafar MS, Othman I. (2009) “Effect of Torsion on Externally Prestressed Segmental Concrete Bridge with Shear Key”, Am. J. Eng. Appl. Sci., vol. 2, no. 1, pp. 54–60.

6. AlGorafi MA, Ali AAA, Jaafar MS, Othman I. (2010) 2010. “Experimental Study of Externally Prestressed Segmental Beam Under Torsion”, Eng. Struct., vol. 32, no. 11, pp. 3528–3538.
7. AlGorafi MA, Ali AAA, Jaafar MS, Othman I. (2011) “Externally Prestressed Monolithic and Segmental Concrete Beams under Torsion”: A Comparative Finite Element Study. OP Conference Series: Materials Science and Engineering, 17, doi:10.1088/1757-899X/17/1/012041
8. AlGorafi MA, Ali AAA, Jaafar MS, Othman I. (2011) “Evaluation of Structural Behavior of Externally Prestressed Segmented Bridge with Shear Key under Torsion”, J. Struct. Eng.vol. 1, no. 1, pp. 28–35.
9. Abdel-Aziz, M.A, (2018). “Behavior of segmental box girders with external prestrsessing under shear and torsion” PH. D Thesis Faculty of engineering, Tanta university.
10. El-Shafiey, T., Khalil, A., Etman, E., Hussein, M., and. Abel-Aziz, M., (2017) . “Segmental Box Girder Bridges with External Prestressing Under Combined Shear, Moment and Torsion”: Review Paper. International Conference on Advances in Structural and Geotechnical Engineering At 27-30 March 2017, Hurghada, Egypt
11. El-Shafiey, T., Khalil, A., Etman, E., Hussein, M., and. Abel-Aziz, M., (2017). “Experimental Investigation on The Behavior of Segmental Box Girder Bridges with External Prestressing Under Combined Shear, Moment and Torsion”. International Conference on Advances in Structural and Geotechnical Engineering 2017 At 27-30 Marc, Hurghada, Egypt
12. El-Shafiey, T., Khalil, A., Etman, E., Hussein, M., and. Abel-Aziz, M., (2018). “Experimental investigation on externally prestressed segmental bridges under torsion using different joints”. International Conference on short and medium span bridges, 2018 At 31 july-3 Quebec City, Canada.
13. AASHTO. (2010). Guide specifications for design and construction of segmental concrete bridges. Washington.
14. Below KD, Hall AS, Rangan BV (1975). “Theory for concrete beams in torsion and bending”. J Struct Eng, ASCE;101:1645–60.
15. Diep B.K. and Umehara H. (2002). “Non-linear analysis of externally prestressed concrete beams”. Electronic Journal of Structural Engineering 2. http://www.ejse.org/.
16. Misic J, Warwaruk J. (1978). “Strength of prestressed solid and hollow beams subjected simultaneously to torsion, shear, and bending”. ACI Struct J; SP55: 515–545.